https://doi.org/10.5194/amt-2020-337
Preprint. Discussion started: 28 September 2020

Atmospheric Measurement Techniques Discussions

Determination of black carbon mass concentration from aerosol light absorption using variable mass absorption cross-section

Weilun Zhao[1], Wangshu Tan[1], Gang Zhao[2], Chuanyang Shen[1], Yingli Yu[1], Chunsheng Zhao[1]

[1]Department of Atmospheric and Oceanic Sciences, School of Physics, Peking University, Beijing 100871, China

[2]State Key Joint Laboratory of Environmental Simulation and Pollution Control, College of Environmental Sciences and Engineering, Peking University, Beijing 100871, China

Correspondence to: Chunsheng Zhao (zcs@pku.edu.cn)

Abstract. Atmospheric black carbon (BC) is the strongest visible solar radiative absorber in the atmosphere, exerting significant influences on the earth's radiation budget. The mass absorption cross-section (MAC) is a crucial parameter for converting light absorption coefficient (σ_{ab}) to mass equivalent BC concentration (m_{BC}). Traditional filter-based instrument, such as AE33, uses a constant MAC of 7.77 m^2/g to derive m_{BC}, which may lead to uncertainty in m_{BC}. In this paper, a new method of converting light absorption coefficient to ~~BC~~ mass concentration is proposed by incorporating the variations of MAC attributed to the influences of aerosol coating state. Mie simulation showed that MAC varied dramatically with different core-shell structures. We compared our new method with traditional method during a field measurement at a site of North China Plain. The results showed that the MAC was smaller (larger) than 7.77 m^2/g for particle smaller (larger) than 280 nm, resulting in BC mass size distribution derived from new method was higher (lower) than traditional method for particle smaller (larger) than 280 nm. Size-integrated BC mass concentration derived from new method was 16% higher than traditional method. Sensitivity analysis indicated that the uncertainty in m_{BC} caused by refractive index (RI) was with in 35% and the imaginary part of RI had dominant influence on the derived m_{BC}. This study emphasizes the necessity to take variations of MAC into account when deriving m_{BC} from σ_{ab} and can help constrain the uncertainty in m_{BC} measurements.

1 Introduction

Black carbon (BC) is an important component of ambient aerosol particles. Because of its highly absorbing properties in the visible spectral region, BC is considered to have a significant influence on global warming. The warming effects of BC is only second to that of carbon dioxide (Ramanathan and Carmichael, 2008). Despite the importance of BC to climate, the global mean direct radiative forcing of BC particles still spans over a poorly constrained range of 0.2 – 1 W/m^2 (Chung et al., 2012;Bond et al., 2013;Boucher et al., 2013). The large uncertainty of BC radiative forcing is partially attributed to the lack of reliable measurements of BC mass concentration in the atmosphere (Arnott et al., 2005;Boucher et al., 2013). Furthermore, BC aerosols can serve as cloud condensation nuclei or ice nucleation particles and change atmospheric convection by heating aerosol layer and influencing the regional precipitation patterns and cloud lifetime (Wild, 2012;Ramanathan and Carmichael, 2008).To fully evaluate the influences of BC particles on solar radiation or precipitation, more precise measurements of BC mass loading in the atmosphere are required.

A variety of techniques have been developed to measure real-time BC mass concentrations. Aethalometer (Hansen et al., 1984), Particle Soot Absorption Photometer (PSAP) (Bond et al., 1999), and Multiple-Angle Absorption Photometer (MAAP) (Petzold

https://doi.org/10.5194/amt-2020-337
Preprint. Discussion started: 28 September 2020

Atmospheric Measurement Techniques Discussions

and Schonlinner, 2004) are based on filter-based attenuation, while the Single Particle Soot Photometer (SP2) is a light-induced incandescent instrument (Stephens et al., 2003;Schwarz et al., 2006). Other instruments that use photo-acoustic methods such as Photoacoustic Spectrometer (PAS) (Truex and Anderson, 1979) or Photo-Acoustic Soot Spectrometer (PASS) have also been introduced. The aethalometer AE33 (model 33, Magee, USA), a convenient and rapid instrument, is commonly used for routine BC observations or dedicated campaigns (Castagna et al., 2019;Sandradewi et al., 2008;Helin et al., 2018). It measures real-time BC concentrations by converting the absorption coefficient (σ_{ab}) into mass equivalent BC concentrations (m_{BC}) through a constant mass absorption cross-section (MAC), which provides the BC absorption per unit mass.

However, it has been reported that the MAC of BC is substantially affected by the process through which BC mixes with other aerosol components (Gunter et al., 1993;Doran et al., 2007;Lack and Cappa, 2010;Peng et al., 2016). Field measurements have indicated that fresh BC particles are generally subject to several coating processes while being transported in the atmosphere and tend to be covered in layers of other organic or inorganic components (Shiraiwa et al., 2007;Cappa et al., 2019;Bond et al., 2006). The gathered shell that builds up on the BC core, acting as a lens to focus additional incident light on the enclosed BC core, can enhance BC light absorption (Fuller et al., 1999) and has significant influences on the BC radiative forcing (Jacobson, 2001). This light absorption enhancement has been termed as "lensing effect" of the BC particles.

For typical core-coating mixed BC containing particles, this lensing effect was found to enhance BC absorption by 50-100% (Bond et al., 2006). Schwarz et al. (2008) found that fresh soot particles internally mixed with sulfates and organics during transportation, and the lensing effect enhanced the light absorption by a factor of 1.3-1.5. Some controlled laboratory studies also confirmed the occurrence of absorption enhancement and their conclusions were consistent with the model calculation (Adler et al., 2010;Brem et al., 2012;Shiraiwa et al., 2010). Meanwhile, other field studies demonstrated a wide range of this lensing effect (Cappa et al., 2019). In contrast, some field observations showed a slight absorption enhancement (Cappa et al., 2012;Nakayama et al., 2014). A wide range of MAC (2-25 m^2/g) has been reported in previous studies (Bond and Bergstrom, 2006;Sharma et al., 2002;Schwarz et al., 2008).

Some studies suggested using site-specific MAC values for converting σ_{ab} into m_{BC} (Martins et al., 1998;Schmid et al., 2006). However, field measurements indicated that MAC showed both large temporal and spatial variability (Bond and Bergstrom, 2006;Lack et al., 2012;Cappa et al., 2012;Ram and Sarin, 2009). Bond and Bergstrom (2006) suggested using consistent MAC and refractive index (RI) values for the BC measurements. In addition to the mixing state, the degree of MAC also relies on diameter of the BC core (D_{BC}), RI, coating thickness, and the location of the BC core (Bond and Bergstrom, 2006;Fuller et al., 1999;Lack and Cappa, 2010). To better determine the current atmospheric BC mass loading, a more reliable MAC application is imperative to infer BC mass from measured light attenuation.

The hypothetical BC mixing state affects the corresponding absorption properties. It is critical to propose a method to infer m_{BC} from light attenuation measurements considering aerosol size and the process by which BC aerosols mix with other aerosol components. A simplified core-shell configuration has been introduced to illustrate the structure of BC-containing particles and calculate the relevant optical properties. Several studies have demonstrated that it is appropriate to use the core-shell configuration

https://doi.org/10.5194/amt-2020-337
Preprint. Discussion started: 28 September 2020

Atmospheric Measurement Techniques Discussions

for aged aerosol (Majdi et al., 2020;Liu et al., 2019;Li et al., 2019).

With the objective of improving the reliability of m_{BC} inferred from AE33, the Mie model incorporated with core-shell configuration hypothesis was applied in this study to assess the limitation of the constant conversion factor used for MAC. Based on the detailed analysis of the relationship among MAC, D_{BC}, and coating thickness (T_{shell}), a modified approach has been proposed for filter-based instruments to derive m_{BC} from σ_{ab}. This modified method measures size-resolvoled m_{BC} accurately and improves the evaluation of BC radiative forcing.

2 Dataset and instrumentation

The measured BC particle mass size distribution (BCPMSD) was obtained from the field campaign conducted at the Zhangqiu Meteorology Station (36°42'N, 117°30'E), Shandong Province. This field campaign lasted for about 1 month, from July 23, 2017 to August 24, 2017. The Zhangqiu observation site is located in the North China Plain (NCP) and is surrounded by farmland and residential areas, representing regional background conditions of the NCP. The DMA (Differential Mobility Analyzer)-SP2 system measurements to determine the number fraction of BC-containing aerosols and to compare AE33 and the three-wavelength photoacoustic soot spectrometer (PASS-3) were conducted in Taizhou (119°57' E, 32°35' N). The suburban measurement site Taizhou lies at the south end of the Jianghuai Plain in the East of China. This industrial area between the two megacities of Nanjing and Shanghai has experienced severe pollution during the past thirty years. The measurements were conducted from May 24, 2018 to June 18, 2018. The measurements for comparing AE33 and PASS-3 were also conducted from March 20, 2018 to April 30, 2018 and from October 10, 2018 to October 19, 2018 in Peking University (39°59' N, 116°18' E). This site is located at the northwest of Beijing, a megacity experiencing severe and complex urban pollution. Meanwhile, from March 21, 2017 to April 9, 2017 at the Peking University site, the results from simultaneous measurements from AE51 (model 51, microAeth, USA) and AE33 were compared.

All the measurements in the three sites were conducted in containers where ambient temperature was controlled within 24 ± 2 °C with a particle pre-impactor to remove particles larger than 10 μm from the input air stream. The drying systems in the three sites were configured with a Nafion dryer to keep the relative humidity of sample flow below 40%. This type of dryer performs good in reducing aerosol losses. The transmission efficiency of the Nafion dryer is up to 90% for particles smaller than 10 nm and rises up to 100% for particles larger than 30 nm (The performance details of the Nafion dryer can be accessed at http://www.permapure.com). During the field campaign at the Zhangqiu site, the particle number size distribution (PNSD) as well as BCPMSD were simultaneously determined using the measurement system developed by (Ning et al., 2013). The instrument setup was further improved by Zhao et al. (2019b). The polydisperse aerosol sample flow was first drawn into DMA (Model 3080, TSI, USA) to select relatively monodispersed aerosol sub-populations with diameters ranging from 97 to 602 nm. Sheath and sample flows were set as 3 and 0.5 L/min, respectively. The selected monodispersed aerosol populations were further divided into two paths. One path (0.2 L/min) was drawn into AE51 for m_{BC} measurements. The other path (0.3 L/min) was analyzed using CPC (model 3772, TSI, USA) for number concentration measurements. As the standard sample flow for CPC is 1 L/min, a cleaned airflow of 0.7 L/min was added for compensation. A BCPMSD cycle measured here required 5 min and we averaged the data with a temporal resolution

https://doi.org/10.5194/amt-2020-337
Preprint. Discussion started: 28 September 2020

Atmospheric Measurement Techniques Discussions

of 2 hours. The dry aerosol scattering coefficients at 525 nm were measured simultaneously by an integrated nephelometer (Ecotech Pty Ltd., Aurora 3000) with a flow rate of 3 L/min. The temporal resolution was 1 min. Similar to the measured BCPMSD, aerosol scattering coefficients that were used to represent air pollution conditions were also averaged with a temporal resolution of 2 hours. While observing BCPMSD at the Beijing site, Zhao et al. (2019b) added AE33 (3 L/min) simultaneously to measure the bulk m_{BC}. The bulk m_{BC} from AE33 and from the integrated BCPMSD measured by AE51 were then compared. For AE51, the influence of loading effect was resolved by using $\sigma_{ab,corrected} = (1 + k \cdot ATN)\sigma_{ab,uncorrected}$. $\sigma_{ab,corrected}$ and $\sigma_{ab,uncorrected}$ are the corrected and uncorrected σ_{ab}, respectively. Factor k was set as 0.004 and ATN is the measured light attenuation when particles load on the fiber filter of AE51. A recommended compensation of 2.6 was introduced here to mitigate the multiple scattering problem (Zhang et al., 2018). Results showed that the variation trends and magnitudes of m_{BC} measured by AE33 and AE51 were in good consistence (Zhao et al., 2019b). Therefore, in this study, the BCPMSD measured by AE51 was regarded as the measurement results of AE33, and the size-resolved σ_{ab} were retrieved by the constant MAC value of 7.77 m^2/g used in AE33.

For the coupling DMA-SP2 system measurement, the dried sample flow was drawn into DMA to select particles with diameters ranging from 200 to 450 nm. Then, the selected monodispersed aerosol samples were analyzed in SP2 (0.12 L/min) to identify the BC containing particles and in CPC (0.28 L/min) to count the total number of particles. The size-resolved number fraction of BC-containing particles was then derived. As the total flowrate was 0.4 L/min from DMA, the sheath flow of DMA was 4 L/min. Detailed configuration of the DMA-SP2 system has been demonstrated in a previous study (Zhao et al., 2019a). According to the measurements from Taizhou, only 17% of the ambient particles that contained BC averagely for bulk aerosol populations.

We adjusted the measured wavelengths of AE33 to the measured wavelengths of PASS-3 (405 nm, 532 nm, and 781 nm). Measurement results from Taizhou and Beijing showed that all the ratios of σ_{ab} measured by AE33 with a measurement flowrate of 3 L/min and PASS-3 with a measurement flowrate of 1 L/min at the three wavelengths varied slightly over the East and North China Plain (± 0.04), with the average value at 2.9. Therefore, as the measurement results between AE33 and AE51 were consistent, all the size-resolved σ_{ab} from AE51 adopted in this study were corrected through the mean ratio of 2.9. All the measurement systems at the three sites are shown in Fig. S1 in the supplement.

3 Method

For current filter-based intruments, m_{BC} are generally derived from σ_{ab} through a constant MAC value. However, the MAC values are enhanced by different degrees when BC particles are mixed with other weakly-absorbing materials, leading to large uncertainties on BC mass retrieval and further evaluations of BC atmospheric optical effects. In order to gain more accurate atmospheric BC mass loading, it is critical to consider the discrepancies in MAC caused by variations in the coating process, BC sizes, etc. Among with the core-shell configuration hypothesis, developing the relationship between MAC, D_{BC}, and T_{shell} is a new approach to correlate m_{BC} with σ_{ab}.

3.1 Core-shell geometry of aerosol particles

To evaluate the theoretical discrepancies in MAC values caused by the corresponding impact factors, an appropriate model simulation is needed for representing a single BC particle's optical properties. There are three widely employed mixing states that

https://doi.org/10.5194/amt-2020-337
Preprint. Discussion started: 28 September 2020


Atmospheric Measurement Techniques Discussions

are used to represent the structure of BC-containing aerosols: internal, external, and core-shell model (Ma et al., 2011;China et al., 2015). Generally, newly-emitted BC particles are chain-like aggregates composed of small spheres. During the coating process, the chain-like BC aggregates become more compact as they collapse and are coated as a core by organic and inorganic materials (Bond and Bergstrom, 2006). Therefore, core-shell configuration is more plausible (Jacobson, 2000). Ma et al. (2012) also indicated that the core-shell assumption can provide a better performance in optical closure than the internal or external models. Furthermore, Moffet et al. (2016) studied particle mixing state and morphology using scanning transmission X-ray microscopy and highlighted that core-shell structure dominated the mixing state of ambient aerosol particles. As aerosols are assumed to be core-shell mixed, with a spherical BC core in the center of the coating sphere, the spherical core and shell favor the Mie model. Therefore, the Mie model was used in this study to simulate the optical properties of BC particles with core-shell mixing state. The consistency in observed and theoretical values obtained using Mie and core-shell morphology support the suitability of this method (Cappa et al., 2012).

3.2 Mie modeled MAC of BC particles

Many optical simulations for BC particles with concentric sphere geometry have been reported and the corresponding results show that the absorption of a pure BC particle will be enhanced when a shell composed of non-absorbing material deposits on this pure BC particle. Since we focused on the optical properties rather than chemical compositions of the mixed aerosols, a simplified hypothesis of BC/sulfate mixtures, which is frequent in the atmosphere (Khalizov et al., 2009), was introduced in the algorithm for calculating m_{BC}.

Since the filter-based instruments (AE33) use σ_{ab} at the wavelength of 880 nm to determine m_{BC}, the MAC distribution for a wide range of core and coating sizes at the wavelength of 880 nm, calculated using the Mie theory, has been presented. The refractive index (RI), reported to vary with incident light wavelength, is an important parameter to determine aerosol optical properties. However, as BC particles can be emitted from different fuels and conditions, RI cannot be observed directly, with both real and imaginary part of RI varying over a significantly wide range. Liu et al. (2018) summarized RI values for specific wavelengths and showed that the real part is generally in the range of 1.5 to 2.0 while the imaginary part usually varies from 0.5 to 1.1 (Sorensen, 2001;Bond and Bergstrom, 2006). Therefore, the real part and imaginary part of RI were set to change from 1.5 to 2.0 and from 0.5 to 1.1, respectively, with a step increase of 0.01. Meanwhile, the RI of sulfate was set as $1.55\text{-}1.0^{-6}$ i and the density of BC was set as 1.8 g/cm^3, similar to Bond et al. (2006). A total of 3111 values were obtained, and the averaged values are illustrated in Fig. 1. The D_{BC} and total aerosol particle diameter ($D_{particle}$, D_{BC} + T_{shell}) ranged from 10 to 700 nm.

Figure 1 presents several features of the variation pattern of MAC. MAC values varied significantly with D_{BC} and the thickness of non-absorbing coating. When the D_{BC} was less than 100 nm, the thickness of the coating dominated the variation of MAC values, and MAC values increased with T_{shell}. As the value T_{shell} increased, the lensing effect became more significant. MAC value can increase from 4 m^2/g to about 17 m^2/g when the total aerosol size reached up to 700 nm. When the D_{BC} was larger than about 100 nm, both T_{shell} and D_{BC} determined MAC values and D_{BC} played a more important role. MAC increased with T_{shell} and decreased with the D_{BC}. Moreover, even for pure BC particles, MAC values varied significantly with the size of BC particles. For smaller

https://doi.org/10.5194/amt-2020-337
Preprint. Discussion started: 28 September 2020

Atmospheric Measurement Techniques Discussions

particles, the MAC values increased slightly with BC size until D_{BC} reached 220 nm. Then, MAC decreased with an increase in D_{BC}. Therefore, the constant MAC value of 7.77 m^2/g used in AE33 is only appropriate for a very limited condition.

3.3 New method to retrieve m_{BC} by considering the variation of MAC

In this subsection, we introduce a new method to determine m_{BC} from the measurement of the σ_{ab} at a given diameter. For a given $D_{particle}$, if D_{BC} is assumed, the corresponding T_{shell} is fixed. Combining the simultaneously measured PNSD and the percentage of particles containing BC, the number of BC-containing particles is then determined at $D_{particle}$. Corresponding absorption properties at the $D_{particle}$ with fixed D_{BC} and T_{shell} can be calculated using the Mie model. Hence, if the number concentration of BC-containing particles and σ_{ab} at a given $D_{particle}$ are measured, we can infer the D_{BC} by closing the measured and the calculated σ_{ab}. Then, the m_{BC} can be obtained from D_{BC} for every $D_{particle}$. Finally, the BCPMSD is derived.

The detailed iterative procedure is illustrated in Fig. 2. As the absorption properties of BC particles in different coating states have been evaluated with the Mie model, as represented in Fig. 1, a simplified algorithm for deriving BCPMSD was proposed by considering Fig. 1 as a look-up table. For every specific $D_{particle}$, if a D_{BC} is assumed, the corresponding MAC of the particle can be derived from the look-up table. Then, the σ_{ab} can be derived from the MAC, the assumed BC density (1.8 g/cm^3 in this study), and the number of BC-containing particles (17% of the total number for every $D_{particle}$). We adjusted the guessed D_{BC} until the difference between calculated and measured σ_{ab} was within an acceptable range (0.1%). Consequently, the D_{BC} and thus the m_{BC} at a given $D_{particle}$ was determined. The m_{BC} at different aerosol sizes were derived separately. Finally, the size-resolved m_{BC} and the bulk m_{BC} were obtained.

It should be pointed out that the retrieval algorithm of BCPMSD is based on the assumption that BC-containing particles of a fixed diameter are all core-shell mixed and the corresponding D_{BC} for a specific $D_{particle}$ is same. Moreover, a constant number percentage (17%) of BC-containing particles was adopted in this study. However, the BC-containing particle fraction varied with the primary source, time, coagulation, and extent of atmospheric process. The influence attributed to the constant fraction of BC-containing particles has been discussed in section 2 of the supplement. Additionally, Bond et al. (2013) summarized the density for different graphitic materials. The density values are 1.8 – 2.1 g/cm^3 for pure graphite, 1.8 – 1.9 g/cm^3 for pressed pellets of BC, and 1.718 g/cm^3 for fullerene soot. A constant density (1.8 g/cm^3) for BC was briefly used to calculate MAC and BC mass from the volume of particles with a diameter of D_{BC}. Therefore, the uncertainty of derived m_{BC} in this study simply depends on the ratio of 1.8 g/cm^3 and the real density. Finally, the MAC values in the look-up table were the averaged values for different RI and the corresponding effects have been discussed in section 5.

4 Results and discussion

Figure 3 provides a comprehensive overview of the variations in measured and retrieved size-resolved parameters during the campaign. As evident from Fig. 3(a), for the BCPMSD derived by the new method, two modes were found, similar to the results of AE33. Figure 4(a) shows the averaged BCPMSD derived from the new method and AE33 during the campaign. The finer mode was located between 97 – 240 nm while the coarser mode was located between 240 – 602 nm. Figure 3(b) represents the relative deviations between the BCPMSD derived from the new proposed method and those derived from a constant MAC value of 7.77

https://doi.org/10.5194/amt-2020-337
Preprint. Discussion started: 28 September 2020


Atmospheric Measurement Techniques Discussions

198 m^2/g. The results indicate that with the boundary of 280 nm, two opposite deviation tendencies exist. For aerosol particles larger
199 than 280 nm, the m_{BC} derived by the new method were mostly lower than those derived with the constant MAC value of 7.77 m^2/g.
200 In contrast, when aerosol particles were smaller than 280 nm, the m_{BC} from the new method were significantly higher than those
201 calculated by the constant MAC, as shown in Fig. 3(c). Figure 3(c) shows the time series of size-resolved MAC during the derivation
202 process of BCPMSD. According to Fig. 3(c), for aerosol particles smaller than 280 nm, the corresponding MAC was almost lower
203 than 7.77 m^2/g. This is because the MAC values of particles smaller than 280 nm are mostly lower than 7.77 m^2/g, as represented
204 in Fig. 1. A smaller MAC implies a weaker absorption ability, which means that the same measured σ_{ab} will correspond to an
205 increased m_{BC}. Therefore, more BC mass loadings were derived from the new method. For aerosol particles larger than 280 nm, in
206 order to match the measured σ_{ab}, the corresponding D_{BC} were generally found to be in those regions of look-up table where the
207 MAC values were larger than 7.77 m^2/g (Fig. 3(c)). Thus, the BC mass loadings for particles larger than 280 nm were found to be
208 less than those calculated with the constant MAC value of 7.77 m^2/g. The simultaneously measured scattering coefficients at 525
209 nm were introduced here to represent air pollution. As shown in Fig. 3(d), the observation station experienced different levels of
210 pollution. Deviations of m_{BC} derived from the newly proposed method and the constant MAC at different aerosol sizes did not show
211 dependencies on pollution conditions.
212 Figure 3(e) shows the time series of m_{BC} at finer and coarser modes. Compared to the results of AE33, the m_{BC} were more
213 concentrated in the finer mode as compared to the coarser mode. The m_{BC} at finer mode were found to be higher than those at the
214 coarser mode for 73% of the experiment duration. The variation trends of bulk m_{BC} calculated by considering the variations of MAC
215 and a constant MAC were similar (Fig. 3(f)). The bulk m_{BC} calculated by the new method were higher than those derived by the
216 constant MAC in 83% of the experiment duration.
217 The m_{BC} calculated from the new method and AE33 for different aerosol size ranges were statistically analyzed. As shown in Fig.
218 4, for all m_{BC} of aerosols ranging between 97 – 602 nm and 97 – 280 nm derived from new method and AE33, strong linear
219 relationships were observed with correlation coefficients of 0.99 and 1.00, respectively. The ratios between the m_{BC} derived from
220 AE33 and the new method for aerosol diameter ranges of 97 – 602 nm and 97 – 280 nm were 0.84 and 0.69, respectively, indicating
221 that the m_{BC} obtained from AE33 was 16% lower for bulk aerosol particles and 31% lower for aerosols smaller than 280 nm. For
222 the diameter range of 280 – 602 nm, MAC values varied significantly and the deviations in m_{BC} derived from the new method and
223 AE33 were divided into two types with a boundary of 0.7 $\mu g/m^3$. If the m_{BC} derived from AE33 was lower than 0.7 $\mu g/m^3$, there
224 was a relatively consistent ratio of 1.13 between the m_{BC} from the new method and AE33, with a correlation coefficient of 0.95.
225 Therefore, BC mass loading from the AE33 algorithm was 13% higher for aerosol particles larger than 280 nm and m_{BC} lower than
226 0.7 $\mu g/m^3$. However, when the m_{BC} derived from AE33 was larger than 0.7 $\mu g/m^3$, data points become discrete, and the relationship
227 between the m_{BC} derived from AE33 and the new method could be expressed through an equation ($y = 0.29 + 0.48x$). However,
228 these comparisons for aerosols at different size ranges were obtained based on the measurements in the NCP. Additionally, the
229 number of samples where m_{BC} of 280 – 602 nm were larger than 0.7 $\mu g/m^3$ was too small. Further studies on BCPMSD in conjunction
230 with the PNSD measurements at different sites need to be carried out.

https://doi.org/10.5194/amt-2020-337
Preprint. Discussion started: 28 September 2020

Atmospheric Measurement Techniques Discussions

5 Influences of RI on MAC

As the RI of BC is still reported to vary over a wide range and the MAC used in this study was a mean value, it is critical to assess the impact caused by the real and imaginary parts on the calculated MAC and the derived BC mass concentrations. For aerosol particles with fixed D_{BC} and T_{shell}, we calculated the MAC of BC with the real part of RI ranging from 1.5 to 2.0 and imaginary part ranging from 0.5 to 1.1. The step increase of both real and imaginary parts was 0.01 and there were 3111 MAC values for every aerosol particle with fixed BC core size and T_{shell}. The ratio of standard deviation to the mean value for these 3111 MAC values have been presented to demonstrate the uncertainty in MAC due to the uncertainty of BC RI.

Figure 5(a) shows the uncertainties in MAC along different values of D_{BC} and T_{shell}. It shows that aerosol particles with a small BC core have larger uncertainties and all the uncertainties were below 24%. When $D_{particle}$ was fixed, the uncertainties decreased with D_{BC}. When D_{BC} was determined, the uncertainties did not change much with T_{shell}. For pure BC particles, the uncertainties also decreased with BC particle size. Figure 5(b) shows the uncertainties when the imaginary part was fixed at 0.8 and the real part ranged from 1.5 to 2.0 with an interval of 0.01. It can be seen that when the imaginary part of RI was fixed, variations in the real part led to slight uncertainties. All the uncertainties were found to be below 14%. Figure 5(c) demonstrates the uncertainties when the real part was fixed at 1.75 and the imaginary part ranged from 0.5 to 1.1 with an interval of 0.01. Comparing Fig. 5(a) and 5(c), we can see that the patterns of MAC uncertainties were similar. Overall, the uncertainties were dominated by the variations of the imaginary part and only slightly affected by variations in the real part.

The variations in on m_{BC} caused by the uncertainties in RI were further evaluated. As stated in section 3.2, all MACs in the look-up table in Fig. 1 are the mean values as the imaginary part and real part of BC RI varied over a wide range. Therefore, the mean MACs in the look-up table plus corresponding standard deviation (MAC + Std) and minus corresponding standard deviation (MAC – Std) were utilized to show the uncertainties in m_{BC} caused by RI of BC. As we can see from Fig. 6(a), irrespective of the MAC values in look-up table were MAC + Std or MAC – Std, there was no change in the mode of BCPMSD. The derived m_{BC} of all aerosols ranging from 97 – 602 nm increased when the MAC values used in the look-up table were MAC – Std and decreased when MAC + Std values were used in the look-up table. Compared to the bulk m_{BC} retrieved through the look-up table with mean MAC, those derived through the look-up table with MAC – Std were higher within 35% (Fig. 6(b)). The decrease in the magnitude of derived m_{BC} caused by MAC + Std values was significantly less than the increase in the magnitude caused by the MAC – Std values. Similarly, for aerosol particles at both finer and coarser modes, the deviations in m_{BC} caused by MAC + Std or MAC – Std were also within 35% (Fig. 6 (c) and Fig. 6 (d)). Meanwhile, the increase in the magnitude of derived σ_{ab} into m_{BC} caused by the MAC-Std values was also significantly higher than the decrease in the magnitude caused by the MAC + Std values. This sensitivity study indicated that the accuracy of the retrieved BCPMSD is sensitive to the accuracy of MAC values in the look-up table, especially when the real MACs are less than the mean MAC values used in the look-up table.

An idealized concentric core-shell model with a spherical BC core fully coated by sulfate was configured to study the MAC of BC aerosols and derive the m_{BC}. However, freshly emitted BC particles were found to normally exist in the form of loose cluster-like aggregates with numerous spherical primary monomers (Liu et al., 2015). Soon after, these aggregates become coated with other

https://doi.org/10.5194/amt-2020-337
Preprint. Discussion started: 28 September 2020


Atmospheric Measurement Techniques Discussions

components and collapsed to a more compact form during the coating process (Zhang et al., 2008;Peng et al., 2016). Therefore, the uncertainty in the idealized core-shell configuration is discussed in section 3 of the supplement.

6 Conclusions

There was a significant variability in the MAC values of BC with the size of BC core and the thickness of coating, which exerted a significant influence on the optical method for measuring m_{BC}. In this study, a new method was proposed to derive m_{BC} while considering the lensing effect of core-shell structure and subsequently the MAC variations of BC.

A look-up table describing the variations of MAC attributed to the coating state and size of BC core was established theoretically using Mie simulation and assuming a core-shell configuration for BC-containing aerosols. Then, the m_{BC} at different aerosol sizes were derived by finding an appropriate BC core configured with a MAC value from the look-up table to close the calculated and measured σ_{ab}.

This newly proposed method was applied to a campaign measurement in the NCP. There were two modes for BCPMSD at the accumulation mode separated by 240 nm. For 73% of the cases, the m_{BC} of the finer mode were larger than those of the coarser mode during the measurement. The m_{BC} derived by the new method were mostly lower than those derived by a constant MAC of 7.77 m^2/g for particles larger than 280 nm, and higher for particles smaller than 280 nm. Similarly, the bulk m_{BC} accumulated from BCPMSD derived from the new method were mostly higher than those derived from a constant MAC of 7.77 m^2/g.

The uncertainty in derived m_{BC} that was caused due to the wide range of RI of the BC core was also studied. The results indicated that the uncertainty of the imaginary part results in larger uncertainties to the MAC as compared to the real part. The relative uncertainty of the derived m_{BC} was within 35%.

This study provides a new way to derive m_{BC} from σ_{ab} for the widely-used filter-based measurements. This research deepens our understanding of the uncertainty in measured m_{BC} caused by the utilization of a constant MAC and illustrates the great necessity to take the variation of MAC into account. The new method improves the measurements of BCPMSD and is further beneficial to the evaluation of BC radiative forcing.

Data availability

The measurement data involved in this study are available upon request to the authors.

Author contributions

CZ determined the main goal of this study. WZ and WT designed the methods. WZ carried them out and prepared the paper with contributions from all co-authors.

Competing interests

The authors declare that they have no conflict of interest.

References

Adler, G., Riziq, A. A., Erlick, C., and Rudich, Y.: Effect of intrinsic organic carbon on the optical properties of fresh diesel soot, Proceedings of the National Academy of Sciences of the United States of America, 107, 6699-6704, 10.1073/pnas.0903311106, 2010.

https://doi.org/10.5194/amt-2020-337
Preprint. Discussion started: 28 September 2020

Atmospheric Measurement Techniques Discussions

297 Arnott, W. P., Hamasha, K., Moosmuller, H., Sheridan, P. J., and Ogren, J. A.: Towards aerosol light-absorption measurements with
298 a 7-wavelength Aethalometer: Evaluation with a photoacoustic instrument and 3-wavelength nephelometer, Aerosol Science and
299 Technology, 39, 17-29, 10.1080/027868290901972, 2005.
300 Bond, T. C., Anderson, T. L., and Campbell, D.: Calibration and intercomparison of filter-based measurements of visible light
301 absorption by aerosols, Aerosol Science and Technology, 30, 582-600, 10.1080/027868299304435, 1999.
302 Bond, T. C., and Bergstrom, R. W.: Light absorption by carbonaceous particles: An investigative review, Aerosol Science and
303 Technology, 40, 27-67, 10.1080/02786820500421521, 2006.
304 Bond, T. C., Habib, G., and Bergstrom, R. W.: Limitations in the enhancement of visible light absorption due to mixing state, J.
305 Geophys. Res.-Atmos., 111, 13, 10.1029/2006jd007315, 2006.
306 Bond, T. C., Doherty, S. J., Fahey, D. W., Forster, P. M., Berntsen, T., DeAngelo, B. J., Flanner, M. G., Ghan, S., Karcher, B., Koch,
307 D., Kinne, S., Kondo, Y., Quinn, P. K., Sarofim, M. C., Schultz, M. G., Schulz, M., Venkataraman, C., Zhang, H., Zhang, S., Bellouin,
308 N., Guttikunda, S. K., Hopke, P. K., Jacobson, M. Z., Kaiser, J. W., Klimont, Z., Lohmann, U., Schwarz, J. P., Shindell, D., Storelvmo,
309 T., Warren, S. G., and Zender, C. S.: Bounding the role of black carbon in the climate system: A scientific assessment, J. Geophys.
310 Res.-Atmos., 118, 5380-5552, 10.1002/jgrd.50171, 2013.
311 Boucher, O., D. Randall, P. Artaxo, C. Bretherton, G. Feingold, P. Forster, V.-M. Kerminen, Y. Kondo, H. Liao, U. Lohmann, P.
312 Rasch, S.K. Satheesh, S. Sherwood, B. Stevens, and Zhang, X. Y.: Clouds and Aerosols. In: Climate Change 2013: The Physical
313 Science Basis. Contribution of Working Group I to the Fifth Assessment Report of the Intergovernmental Panel on Climate Change,
314 in, edited by: Stocker, T. F., D. Qin, G.-K. Plattner, M. Tignor, S.K. Allen, J. Boschung, A. Nauels, Y. Xia, V. Bex and P.M. Midgley,
315 Cambridge University Press, Cambridge, United Kingdom and New York, NY, USA, 571-657, 2013.
316 Brem, B. T., Gonzalez, F. C. M., Meyers, S. R., Bond, T. C., and Rood, M. J.: Laboratory-Measured Optical Properties of Inorganic
317 and Organic Aerosols at Relative Humidities up to 95%, Aerosol Science and Technology, 46, 178-190,
318 10.1080/02786826.2011.617794, 2012.
319 Cappa, C. D., Onasch, T. B., Massoli, P., Worsnop, D. R., Bates, T. S., Cross, E. S., Davidovits, P., Hakala, J., Hayden, K. L., Jobson,
320 B. T., Kolesar, K. R., Lack, D. A., Lerner, B. M., Li, S. M., Mellon, D., Nuaaman, I., Olfert, J. S., Petaja, T., Quinn, P. K., Song, C.,
321 Subramanian, R., Williams, E. J., and Zaveri, R. A.: Radiative Absorption Enhancements Due to the Mixing State of Atmospheric
322 Black Carbon, Science, 337, 1078-1081, 10.1126/science.1223447, 2012.
323 Cappa, C. D., Zhang, X. L., Russell, L. M., Collier, S., Lee, A. K. Y., Chen, C. L., Betha, R., Chen, S. J., Liu, J., Price, D. J., Sanchez,
324 K. J., McMeeking, G. R., Williams, L. R., Onasch, T. B., Worsnop, D. R., Abbatt, J., and Zhang, Q.: Light absorption by ambient
325 black and brown carbon and its dependence on black carbon coating state for two California, USA, cities in winter and summer, J.
326 Geophys. Res.-Atmos., 124, 1550-1577, 10.1029/2018jd029501, 2019.
327 Castagna, J., Calvello, M., Esposito, F., and Pavese, G.: Analysis of equivalent black carbon multi-year data at an oil pre-treatment
328 plant: Integration with satellite data to identify black carbon transboundary sources, Remote Sens. Environ., 235, 10,
329 10.1016/j.rse.2019.111429, 2019.

https://doi.org/10.5194/amt-2020-337
Preprint. Discussion started: 28 September 2020


Atmospheric Measurement Techniques Discussions

China, S., Scarnato, B., Owen, R. C., Zhang, B., Ampadu, M. T., Kumar, S., Dzepina, K., Dziobak, M. P., Fialho, P., Perlinger, J. A., Hueber, J., Helmig, D., Mazzoleni, L. R., and Mazzoleni, C.: Morphology and mixing state of aged soot particles at a remote marine free troposphere site: Implications for optical properties, Geophys. Res. Lett., 42, 1243-1250, 10.1002/2014gl062404, 2015.

Chung, C. E., Ramanathan, V., and Decremer, D.: Observationally constrained estimates of carbonaceous aerosol radiative forcing, Proceedings of the National Academy of Sciences of the United States of America, 109, 11624-11629, 10.1073/pnas.1203707109, 2012.

Doran, J. C., Barnard, J. C., Arnott, W. P., Cary, R., Coulter, R., Fast, J. D., Kassianov, E. I., Kleinman, L., Laulainen, N. S., Martin, T., Paredes-Miranda, G., Pekour, M. S., Shaw, W. J., Smith, D. F., Springston, S. R., and Yu, X. Y.: The T1-T2 study: evolution of aerosol properties downwind of Mexico City, Atmospheric Chemistry and Physics, 7, 1585-1598, 10.5194/acp-7-1585-2007, 2007.

Fuller, K. A., Malm, W. C., and Kreidenweis, S. M.: Effects of mixing on extinction by carbonaceous particles, J. Geophys. Res.-Atmos., 104, 15941-15954, 10.1029/1998jd100069, 1999.

Gunter, R. L., Hansen, A. D. A., Boatman, J. F., Bodhaine, B. A., Schnell, R. C., and Garvey, D. M.: Airborne measurement of aerosol optical-properties over south-central New-Mexico, Atmospheric Environment Part a-General Topics, 27, 1363-1368, 10.1016/0960-1686(93)90262-w, 1993.

Hansen, A. D. A., Rosen, H., and Novakov, T.: The aethalometer - an instrument for the real-time measurement of optical-absorption by aerosol-particles, Sci. Total Environ., 36, 191-196, 10.1016/0048-9697(84)90265-1, 1984.

Helin, A., Niemi, J. V., Virkkula, A., Pirjola, L., Teinila, K., Backman, J., Aurela, M., Saarikoski, S., Ronkko, T., Asmi, E., and Timonen, H.: Characteristics and source apportionment of black carbon in the Helsinki metropolitan area, Finland, Atmospheric Environment, 190, 87-98, 10.1016/j.atmosenv.2018.07.022, 2018.

Jacobson, M. Z.: A physically-based treatment of elemental carbon optics: Implications for global direct forcing of aerosols, Geophys. Res. Lett., 27, 217-220, 10.1029/1999gl010968, 2000.

Jacobson, M. Z.: Strong radiative heating due to the mixing state of black carbon in atmospheric aerosols, Nature, 409, 695-697, 10.1038/35055518, 2001.

Khalizov, A. F., Xue, H. X., Wang, L., Zheng, J., and Zhang, R. Y.: Enhanced light absorption and scattering by carbon soot aerosol internally mixed with sulfuric acid, Journal of Physical Chemistry A, 113, 1066-1074, 10.1021/jp807531n, 2009.

Lack, D. A., and Cappa, C. D.: Impact of brown and clear carbon on light absorption enhancement, single scatter albedo and absorption wavelength dependence of black carbon, Atmospheric Chemistry and Physics, 10, 4207-4220, 10.5194/acp-10-4207-2010, 2010.

Lack, D. A., Langridge, J. M., Bahreini, R., Cappa, C. D., Middlebrook, A. M., and Schwarz, J. P.: Brown carbon and internal mixing in biomass burning particles, Proceedings of the National Academy of Sciences of the United States of America, 109, 14802-14807, 10.1073/pnas.1206575109, 2012.

Li, Z. J., Tan, H. B., Zheng, J., Liu, L., Qin, Y. M., Wang, N., Li, F., Li, Y. J., Cai, M. F., Ma, Y., and Chan, C. K.: Light absorption properties and potential sources of particulate brown carbon in the Pearl River Delta region of China, Atmospheric Chemistry and

https://doi.org/10.5194/amt-2020-337
Preprint. Discussion started: 28 September 2020

Physics, 19, 11669-11685, 10.5194/acp-19-11669-2019, 2019.

Liu, C., Yin, Y., Hu, F. C., Jin, H. C., and Sorensen, C. M.: The effects of monomer size distribution on the radiative properties of black carbon aggregates, Aerosol Science and Technology, 49, 928-940, 10.1080/02786826.2015.1085953, 2015.

Liu, C., Chung, C. E., Yin, Y., and Schnaiter, M.: The absorption Angstrom exponent of black carbon: from numerical aspects, Atmospheric Chemistry and Physics, 18, 6259-6273, 10.5194/acp-18-6259-2018, 2018.

Liu, H., Pan, X. L., Wu, Y., Wang, D. W., Tian, Y., Liu, X. Y., Lei, L., Sun, Y. L., Fu, P. Q., and Wang, Z. F.: Effective densities of soot particles and their relationships with the mixing state at an urban site in the Beijing megacity in the winter of 2018, Atmospheric Chemistry and Physics, 19, 14791-14804, 10.5194/acp-19-14791-2019, 2019.

Ma, N., Zhao, C. S., Nowak, A., Muller, T., Pfeifer, S., Cheng, Y. F., Deng, Z. Z., Liu, P. F., Xu, W. Y., Ran, L., Yan, P., Gobel, T., Hallbauer, E., Mildenberger, K., Henning, S., Yu, J., Chen, L. L., Zhou, X. J., Stratmann, F., and Wiedensohler, A.: Aerosol optical properties in the North China Plain during HaChi campaign: an in-situ optical closure study, Atmospheric Chemistry and Physics, 11, 5959-5973, 10.5194/acp-11-5959-2011, 2011.

Ma, N., Zhao, C. S., Muller, T., Cheng, Y. F., Liu, P. F., Deng, Z. Z., Xu, W. Y., Ran, L., Nekat, B., van Pinxteren, D., Gnauk, T., Mueller, K., Herrmann, H., Yan, P., Zhou, X. J., and Wiedensohler, A.: A new method to determine the mixing state of light absorbing carbonaceous using the measured aerosol optical properties and number size distributions, Atmospheric Chemistry and Physics, 12, 2381-2397, 10.5194/acp-12-2381-2012, 2012.

Majdi, M., Kim, Y., Turquety, S., and Sartelet, K.: Impact of mixing state on aerosol optical properties during severe wildfires over the Euro-Mediterranean region, Atmospheric Environment, 220, 11, 10.1016/j.atmosenv.2019.117042, 2020.

Martins, J. V., Artaxo, P., Liousse, C., Reid, J. S., Hobbs, P. V., and Kaufman, Y. J.: Effects of black carbon content, particle size, and mixing on light absorption by aerosols from biomass burning in Brazil, J. Geophys. Res.-Atmos., 103, 32041-32050, 10.1029/98jd02593, 1998.

Moffet, R. C., O'Brien, R. E., Alpert, P. A., Kelly, S. T., Pham, D. Q., Gilles, M. K., Knopf, D. A., and Laskin, A.: Morphology and mixing of black carbon particles collected in central California during the CARES field study, Atmospheric Chemistry and Physics, 16, 14515-14525, 10.5194/acp-16-14515-2016, 2016.

Nakayama, T., Ikeda, Y., Sawada, Y., Setoguchi, Y., Ogawa, S., Kawana, K., Mochida, M., Ikemori, F., Matsumoto, K., and Matsumi, Y.: Properties of light-absorbing aerosols in the Nagoya urban area, Japan, in August 2011 and January 2012: Contributions of brown carbon and lensing effect, J. Geophys. Res.-Atmos., 119, 12721-12739, 10.1002/2014jd021744, 2014.

Ning, Z., Chan, K. L., Wong, K. C., Westerdahl, D., Mocnik, G., Zhou, J. H., and Cheung, C. S.: Black carbon mass size distributions of diesel exhaust and urban aerosols measured using differential mobility analyzer in tandem with Aethalometer, Atmospheric Environment, 80, 31-40, 10.1016/j.atmosenv.2013.07.037, 2013.

Peng, J. F., Hu, M., Guo, S., Du, Z. F., Zheng, J., Shang, D. J., Zamora, M. L., Zeng, L. M., Shao, M., Wu, Y. S., Zheng, J., Wang, Y., Glen, C. R., Collins, D. R., Molina, M. J., and Zhang, R. Y.: Markedly enhanced absorption and direct radiative forcing of black carbon under polluted urban environments, Proceedings of the National Academy of Sciences of the United States of America, 113,

https://doi.org/10.5194/amt-2020-337
Preprint. Discussion started: 28 September 2020

4266-4271, 10.1073/pnas.1602310113, 2016.

Petzold, A., and Schonlinner, M.: Multi-angle absorption photometry - a new method for the measurement of aerosol light absorption and atmospheric black carbon, Journal of Aerosol Science, 35, 421-441, 10.1016/j.jaerosci.2003.09.005, 2004.

Ram, K., and Sarin, M. M.: Absorption Coefficient and Site-Specific Mass Absorption Efficiency of Elemental Carbon in Aerosols over Urban, Rural, and High-Altitude Sites in India, Environmental Science & Technology, 43, 8233-8239, 10.1021/es9011542, 2009.

Ramanathan, V., and Carmichael, G.: Global and regional climate changes due to black carbon, Nature Geoscience, 1, 221-227, 10.1038/ngeo156, 2008.

Sandradewi, J., Prevot, A. S. H., Szidat, S., Perron, N., Alfarra, M. R., Lanz, V. A., Weingartner, E., and Baltensperger, U.: Using aerosol light absorption measurements for the quantitative determination of wood burning and traffic emission contributions to particulate matter, Environmental Science & Technology, 42, 3316-3323, 10.1021/es702253m, 2008.

Schmid, O., Artaxo, P., Arnott, W. P., Chand, D., Gatti, L. V., Frank, G. P., Hoffer, A., Schnaiter, M., and Andreae, M. O.: Spectral light absorption by ambient aerosols influenced by biomass burning in the Amazon Basin. I: Comparison and field calibration of absorption measurement techniques, Atmospheric Chemistry and Physics, 6, 3443-3462, 10.5194/acp-6-3443-2006, 2006.

Schwarz, J. P., Gao, R. S., Fahey, D. W., Thomson, D. S., Watts, L. A., Wilson, J. C., Reeves, J. M., Darbeheshti, M., Baumgardner, D. G., Kok, G. L., Chung, S. H., Schulz, M., Hendricks, J., Lauer, A., Karcher, B., Slowik, J. G., Rosenlof, K. H., Thompson, T. L., Langford, A. O., Loewenstein, M., and Aikin, K. C.: Single-particle measurements of midlatitude black carbon and light-scattering aerosols from the boundary layer to the lower stratosphere, J. Geophys. Res.-Atmos., 111, 15, 10.1029/2006jd007076, 2006.

Schwarz, J. P., Spackman, J. R., Fahey, D. W., Gao, R. S., Lohmann, U., Stier, P., Watts, L. A., Thomson, D. S., Lack, D. A., Pfister, L., Mahoney, M. J., Baumgardner, D., Wilson, J. C., and Reeves, J. M.: Coatings and their enhancement of black carbon light absorption in the tropical atmosphere, J. Geophys. Res.-Atmos., 113, 10, 10.1029/2007jd009042, 2008.

Sharma, S., Brook, J. R., Cachier, H., Chow, J., Gaudenzi, A., and Lu, G.: Light absorption and thermal measurements of black carbon in different regions of Canada, J. Geophys. Res.-Atmos., 107, 11, 10.1029/2002jd002496, 2002.

Shiraiwa, M., Kondo, Y., Moteki, N., Takegawa, N., Miyazaki, Y., and Blake, D. R.: Evolution of mixing state of black carbon in polluted air from Tokyo, Geophys. Res. Lett., 34, 5, 10.1029/2007gl029819, 2007.

Shiraiwa, M., Kondo, Y., Iwamoto, T., and Kita, K.: Amplification of Light Absorption of Black Carbon by Organic Coating, Aerosol Science and Technology, 44, 46-54, 10.1080/02786820903357686, 2010.

Sorensen, C. M.: Light scattering by fractal aggregates: A review, Aerosol Science and Technology, 35, 648-687, 10.1080/027868201316900007, 2001.

Stephens, M., Turner, N., and Sandberg, J.: Particle identification by laser-induced incandescence in a solid-state laser cavity, Appl. Optics, 42, 3726-3736, 10.1364/ao.42.003726, 2003.

Truex, T. J., and Anderson, J. E.: Mass monitoring of carbonaceous aerosols with a spectrophone, Atmospheric Environment, 13, 507-509, 10.1016/0004-6981(79)90143-4, 1979.

https://doi.org/10.5194/amt-2020-337
Preprint. Discussion started: 28 September 2020

Atmospheric Measurement Techniques Discussions

Wild, M.: Englightening global dimming and brightening, Bulletin of the American Meteorological Society, 93, 27-37, 10.1175/bams-d-11-00074.1, 2012.

Zhang, R. Y., Khalizov, A. F., Pagels, J., Zhang, D., Xue, H. X., and McMurry, P. H.: Variability in morphology, hygroscopicity, and optical properties of soot aerosols during atmospheric processing, Proceedings of the National Academy of Sciences of the United States of America, 105, 10291-10296, 10.1073/pnas.0804860105, 2008.

Zhang, Y. X., Zhang, Q., Cheng, Y. F., Su, H., Li, H. Y., Li, M., Zhang, X., Ding, A. J., and He, K. B.: Amplification of light absorption of black carbon associated with air pollution, Atmospheric Chemistry and Physics, 18, 9879-9896, 10.5194/acp-18-9879-2018, 2018.

Zhao, G., Tan, T. Y., Zhao, W. L., Guo, S., Tian, P., and Zhao, C. S.: A new parameterization scheme for the real part of the ambient urban aerosol refractive index, Atmospheric Chemistry and Physics, 19, 12875-12885, 10.5194/acp-19-12875-2019, 2019a.

Zhao, G., Tao, J. C., Kuang, Y., Shen, C. Y., Yu, Y. L., and Zhao, C. S.: Role of black carbon mass size distribution in the direct aerosol radiative forcing, Atmospheric Chemistry and Physics, 19, 13175-13188, 10.5194/acp-19-13175-2019, 2019b.

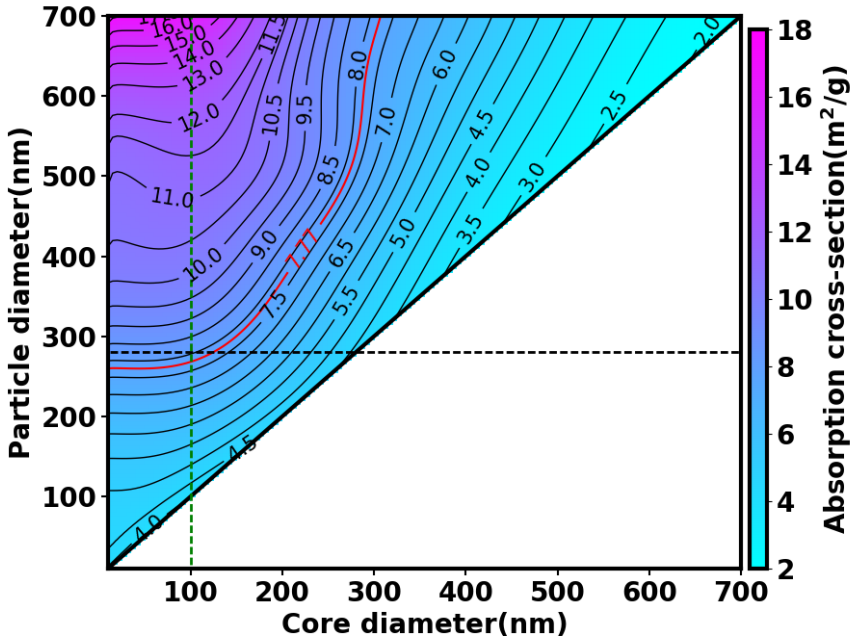

Figure 1. Variations in MAC as a function of D_{BC} and $D_{particle}$, calculated by the concentric core-shell Mie model at the wavelength of 880 nm. The red solid line is the constant MAC value used in AE33. The bold black solid line is the 1:1 line that presents the variations in MAC for pure BC particles with different D_{BC}. The horizontal black dashed line distinguishes particles with a diameter of 280 nm while the vertical green dashed line indicates a D_{BC} of 100 nm.

https://doi.org/10.5194/amt-2020-337
Preprint. Discussion started: 28 September 2020

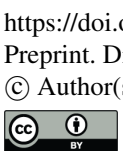

Atmospheric Measurement Techniques Discussions

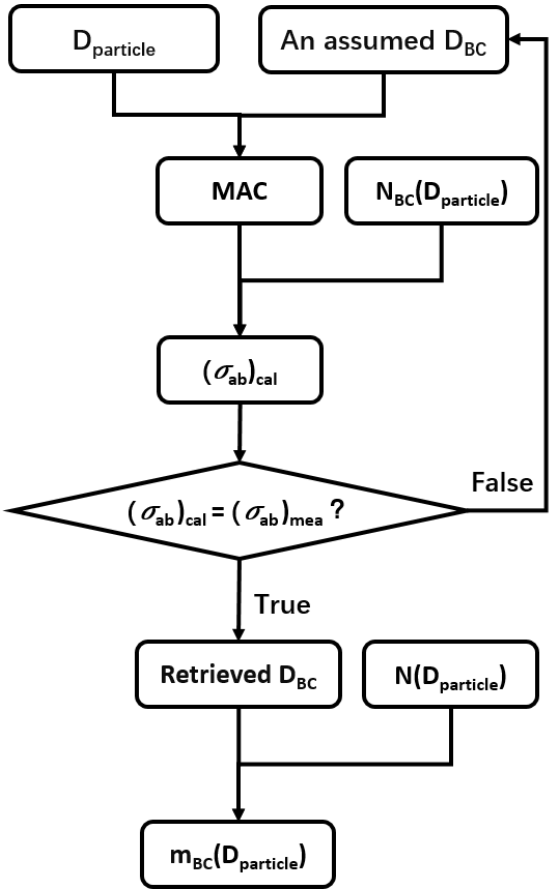

Figure 2. Schematic diagram of the iterative algorithm for retrieving the m_{BC} at a fixed particle diameter based on the look-up table of MAC, particle size and core size. $(\sigma_{ab})_{cal}$ and $(\sigma_{ab})_{mea}$ represent calculated and measured absorption coefficients, respectively. $N_{BC}(D_{particle})$ indicates the number concentration of particle containing BC at the given $D_{particle}$.

https://doi.org/10.5194/amt-2020-337
Preprint. Discussion started: 28 September 2020

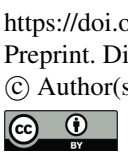

Atmospheric Measurement Techniques Discussions

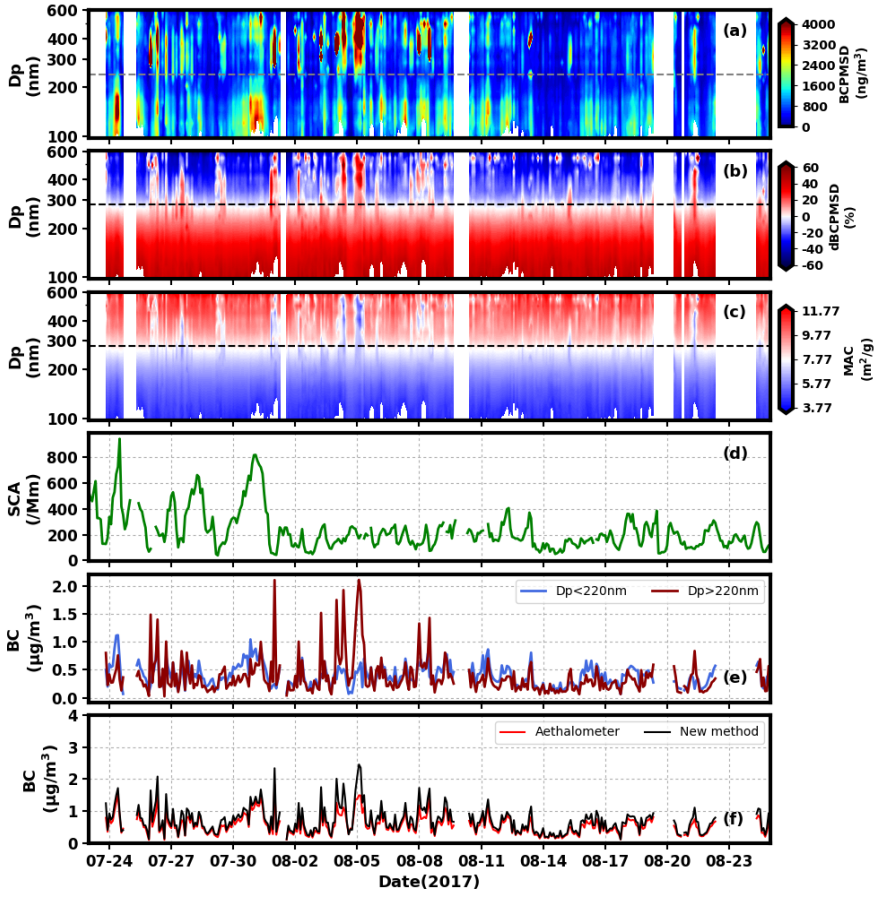

Figure 3. Time series of (a) the BCPMSD derived from the newly proposed method (dashed line indicates the particle size of 240 nm); (b) relative deviations between BCPMSD derived from the new method and a constant MAC of 7.77 m^2/g (dashed line indicates the particle size of 280 nm); (c) the size-resolved MAC determined during the process of retrieving BCPMSD (dashed line indicates the particle size of 280 nm); (d) the scattering coefficients simultaneously measured with the size-resolved σ_{ab}; (e) the m_{BC} for particles smaller than 280 nm and larger than 280 nm; and (f) the m_{BC} determined by the new method and the constant MAC of 7.77 m^2/g.

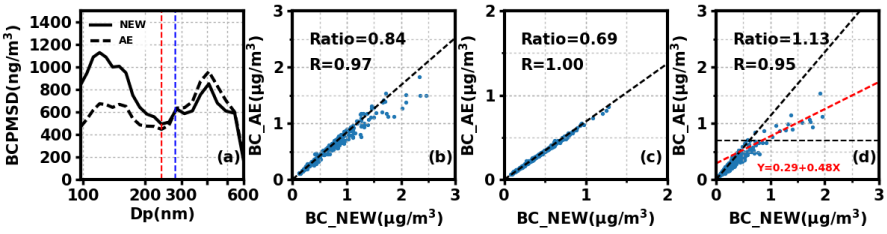

Figure 4. Comparison between the newly proposed method and using a constant MAC of 7.77 m^2/g in the derived results of (a) the BCPMSD (the dashed black line shows the results of AE33 while the solid black line represents the results from the new method; the dashed red line represents the split line (diameter of 240 nm) between finer mode and coarser mode for

https://doi.org/10.5194/amt-2020-337
Preprint. Discussion started: 28 September 2020

Atmospheric Measurement Techniques Discussions

BCPMSD; the dashed blue line indicates the split line (280 nm of diameter) between the opposite tendencies of deviations in the m_{BC} calculated from the new method and the aethalometer); (b) the bulk m_{BC} for particles ranging from 97 nm to 602 nm; (c) the m_{BC} for the finer mode (97 – 280 nm); (d) the m_{BC} for the coarser mode (280 – 606 nm); the dashed black line represents boundary of 0.7 μg/m^3 and the red dashed line is the regression line of the m_{BC} derived from AE and the new method when m_{BC} is larger than 0.7 μg/m^3.

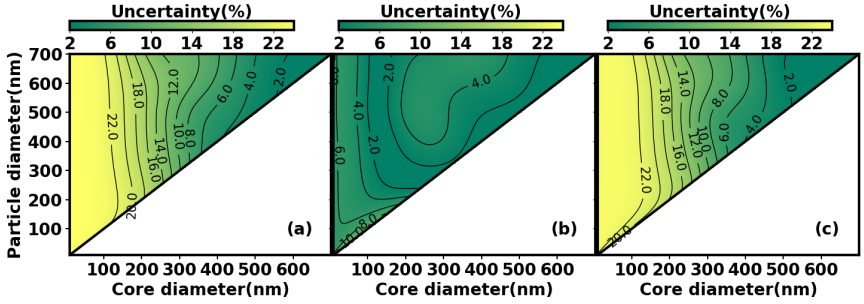

Figure 5. Uncertainty in MAC of BC when (a) real part of RI ranges from 1.5 to 2.0 and imaginary part ranges from 0.5 to 1.1; (b) real part of RI ranges from 1.5 to 2.0 and imaginary part is fixed at 0.8 and (c) real part of RI is fixed at 1.75 and imaginary part ranges from 0.5 to 1.1. The bold black solid line is the 1:1 line and presents the uncertainty of MAC for pure BC particles with different RI.

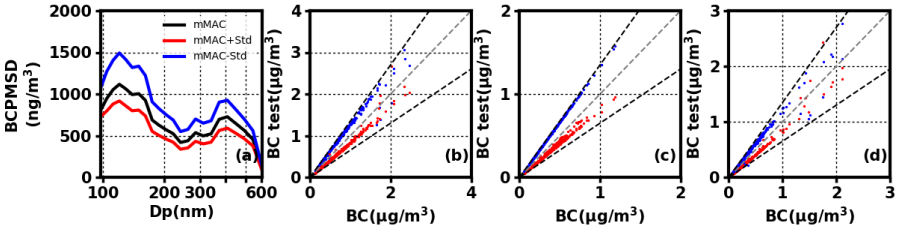

Figure 6. (a) The BCPMSD calculated by using the look up table with mean MAC (black line), mean MAC plus the corresponding standard deviation (red line) and mean MAC minus the corresponding standard deviation (blue line); the m_{BC} derived by the look up table with mean MAC versus those derived by the look up table with mean MAC plus standard deviation (red dots) or mean MAC minus standard deviation (blue dots) for (b) aerosol particles ranging from 97–602 nm; (c) aerosol particles ranging from 97–240 nm (finer mode); and (d) aerosol particles ranging from 240–602 nm (coarser mode). The dashed black line represents the 35% deviation from the 1:1 line (dashed grey lines).